

A laboratory apparatus for the measurement of optical extinction coefficients of postflame soot in the infrared

John F. Widmann,^{a)} Jiann C. Yang, and Matthew Bundy

Fire Research Division, National Institute of Standards and Technology, 100 Bureau Drive, Stop 8663, Gaithersburg, Maryland 20899-8663

Benjamin K. Tsai

Optical Technology Division, National Institute of Standards and Technology, 100 Bureau Drive, Stop 8441, Gaithersburg, Maryland 20899-8441

George W. Mulholland

Fire Research Division, National Institute of Standards and Technology, 100 Bureau Drive, Stop 8663, Gaithersburg, Maryland 20899-8663

(Received 15 July 2002; accepted 25 October 2002)

An experimental apparatus for the measurement of optical extinction coefficients of postflame soot aerosol in the infrared region of the electromagnetic spectrum is presented. Reproducible soot aerosol is generated using a laminar diffusion burner, and the mass concentration of the aerosol is determined gravimetrically. The instrument, which utilizes an infrared spectrograph for the extinction measurements, provides data over the wavelength range 2.5–5.0 μm . The infrared spectrograph, which provides a near-instantaneous measurement of the incident radiation over a range of wavelengths, is ideal for applications in which the deposition of soot over time on the optical windows can interfere with the measurement. Furthermore, the wavelength dependence of the extinction coefficient can be determined independently of the gravimetric measurements, which represents the dominant source of uncertainty in the measurement of the mass specific extinction coefficient. The spectrograph reported herein has been characterized using a well-characterized sodium heat pipe blackbody, and the responsivity of the instrument has been quantified as a function of wavelength. [DOI: 10.1063/1.1533102]

I. INTRODUCTION

Accurate determination of the optical properties of soot aerosol are essential for the interpretation of laser-based diagnostic measurements and the prediction of radiation transport through smoke. For example, the Fire Dynamics Simulator developed at the National Institute of Standards and Technology is used to predict large-scale fire phenomena^{1,2} in a wide variety of fire scenarios. However, to include the effect of radiation transport through smoke filled enclosures on the fire dynamics it is necessary to provide optical characteristics of the soot aerosol. Numerous studies of the optical extinction coefficients of soot particles in the visible and near-infrared regions of the electromagnetic spectrum have been conducted;^{3–8} however, such measurements have not been obtained in the mid-infrared. Radiative heat transfer within fires is dominated by radiation transport over the wavelength range from 2 to 5 μm , and thus the accurate measurement of soot optical properties in this range is critical for the prediction of fire phenomena. This article provides a detailed description of a facility that can be used to obtain such measurements.

The transmission T of radiation through an aerosol dispersion can be quantified using the expression

$$T = \frac{I}{I_0} = \exp(-\sigma_s m_s L) = \exp\left(-K_e \frac{f_v}{\lambda} L\right), \quad (1)$$

where I_0 and I correspond to the incident and transmitted intensities, respectively. Here, σ_s is the mass specific extinction coefficient, m_s is the mass of aerosol per unit volume, and L is the path length. In general, σ_s may be a function of the radiation wavelength λ , and the aerosol properties (chemical composition, temperature, morphology, and size distribution). Accurate knowledge of σ_s permits measurements of m_s using nonintrusive laser extinction techniques provided the particle size dependence of σ_s is neglected and the aerosol dispersion is assumed homogeneous along the path length. Furthermore, reliable values for σ_s are required to include the effect of particulates in radiation transport calculations in fires and combustion systems. The second expression in Eq. (1) is expressed in terms of the soot volume fraction f_v and the dimensionless extinction coefficient. This form is widely used for radiative heat transfer calculations. The two extinction coefficients are related by

$$K_e = \sigma_s \lambda \rho_s, \quad (2)$$

where ρ_s is the density of the condensed phase.

II. EXPERIMENTAL APPARATUS

The experimental apparatus, presented in Fig. 1, consists of a flow control system, a laminar diffusion burner, a black-

^{a)}Author to whom correspondence should be addressed; electronic mail: widmann@nist.gov

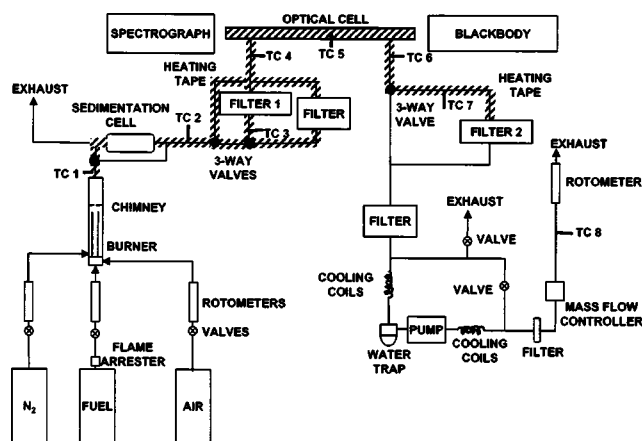


FIG. 1. Schematic of the experimental apparatus.

body source, and an infrared spectrograph to quantify the extinction of radiation due to the aerosol. The soot is generated in the burner, diluted with nitrogen, and carried by the combustion gases and N_2 to the optical cell. The apparatus is equipped with a number of filters to remove particulates from the gas stream prior to the measurement, or to measure gravimetrically the mass of soot aerosol present upstream and downstream of the optical cell. An optional sedimentation cell is also in line to remove the largest soot agglomerates from the aerosol. The sedimentation cell is to reduce soot deposition in the optical cell and associated tubing. Downstream of the optical cell, the particulate is filtered from the gas stream prior to the gas entering the pump. A mass flow controller is used to regulate the gas flow rate through the apparatus.

The laminar diffusion burner consists of two concentric tubes, with fuel and air flowing through the inner and outer tubes, respectively. The data presented here correspond to experiments in which ethene was used as the fuel. The inner diameters of the fuel and air tubes are 9 and 35 mm, respectively. The combustion products flow through a Pyrex⁹ tube with an inner diameter of 26 mm that extends 27 cm downstream of the fuel and air ducts. An outer Pyrex tube surrounds the 27 cm long Pyrex tube as shown in Fig. 1. This tube has an inner diameter of 50 mm and extends 61 cm downstream of the fuel and air ducts. Nitrogen is added between the inner and outer Pyrex tubes to dilute the aerosol downstream of the inner Pyrex tube (see Fig. 1). A tripper plate located 30 cm downstream of the fuel and air ducts is used to instigate turbulent mixing to produce a more homogeneous aerosol dispersion.

The data presented here correspond to fuel and air flow rates of 6.2 and $87.4 \text{ cm}^3 \text{ s}^{-1}$, respectively. The N_2 diluent flow rate was maintained at $221 \text{ cm}^3 \text{ s}^{-1}$, and the flow rate of combustion gases through the optical cell was fixed at $11.1 \text{ cm}^3 \text{ s}^{-1}$. The experimental conditions correspond to a global equivalence ratio (actual fuel-air ratio divided by the stoichiometric fuel-air ratio) of 1.0.

The combustion gases and N_2 diluent transport the particulate to the optical cell, where the extinction measurements are obtained. The Pyrex optical cell has a 25 mm inner diameter and a path length of $L = 38$ cm between the win-

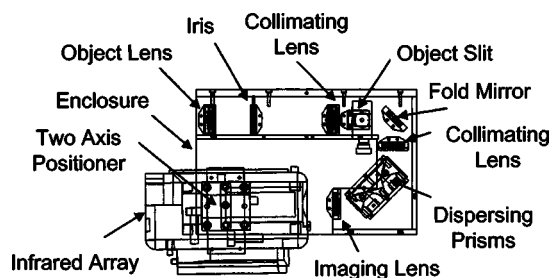


FIG. 2. Schematic of the infrared spectrograph.

dows. Calcium fluoride windows are used on the ends of the optical cell due to the superior transmission characteristics of CaF_2 in this wavelength range. The optical cell is wrapped with resistive heating tape, and the temperature is maintained at 50°C to prevent moisture condensation and minimize thermophoretic deposition of soot particles on the tube wall.

The extinction measurements are obtained by comparing the transmission of radiation through the optical cell with and without soot aerosol present. A blackbody is used to provide radiation with a well-characterized distribution of spectral intensity. The intensity of the radiation is measured as a function of wavelength using a unique imaging spectrograph. The spectrograph contains a two-dimensional PtSi charge coupled device (CCD) array. The 320×244 element array is situated in a Stirling cooled package, and the temperature of the array is maintained at 77 K. A personal computer with an ITI⁹ frame grabber board (12-bit resolution) was implemented to acquire and store the raw pixel voltages. The CCD array was combined with the necessary optics to obtain spectral information along one axis of the two-dimensional array and spatial information along the other axis.

The imaging system of the spectrograph, shown in Fig. 2, is comprised of two independent optical subsystems: a telescope and a prism spectrograph. The telescope consists of an object lens and a collimating lens. A 50 mm object located 500 mm from the first lens results in a 9.6 mm image located 30 mm behind the last lens. A slit is placed at this intermediate image. The resulting exit pupil of the telescope matches the entrance pupil of the prism spectrograph. An object lens and two collimating lenses to one side of the dispersing elements image light from a line source approximately 35 mm in length. To control the size of the source, an iris and a slit are implemented as shown in Fig. 2. A fold mirror is used to reduce the size of the package. An imaging lens focuses the spectrally dispersed image of the line source onto the infrared array detector. The four lens assemblies are combination germanium-silicon achromatic lenses. Using the prism spectrograph consisting of three CaF_2 prisms between the two achromatic doublets, an $f/6$ beam in image space results, and provides the dispersion necessary to spread the $1.9\text{--}5.0 \mu\text{m}$ spectrum across the 7.3 mm short axis of the detector array. The cooled PtSi detector array, which consists of $30 \mu\text{m}$ square pixels, is mounted on a two-axis positioning stage to allow for optimal alignment.¹⁰ Although the spectrograph has been used for radiation emission measurements,¹¹ this instrument has not been used previously in transmission mode in

an aerosol-laden environment for extinction measurements.

The calculation of the mass specific extinction coefficient σ_s requires the determination of the concentration on a mass basis of the aerosol dispersion m_s , as shown in Eq. (1). The mass concentration of particulate in the optical cell is determined gravimetrically by alternately collecting the soot on membrane filters upstream and downstream of the optical cell. The filters used for the gravimetric measurements are labeled filter 1 and filter 2 in Fig. 1. Further characterization of the soot aerosol (size distribution, fractal dimension, and primary particle size) can be performed using transmission electron microscopy.

III. SPECTROGRAPH CHARACTERIZATION

Characterization of the spectrograph was performed using a sodium heat-pipe blackbody (Na-HPBB). The main inconel cavity of the Na-HPBB is 22 mm in diameter. Surrounding the cylindrical cavity is a 90 mm diam tube, which contains the sodium liquid/vapor mixture. A condensing tube at the rear of the blackbody allows the metal vapor to condense, and also serves as the conduit through which the tube is pressurized with helium. The temperature of the Na-HPBB, which is measured with a gold-platinum thermocouple, is computer-controlled by regulating the pressure of the helium. The Au/Pt thermocouple links the Na-HPBB temperature to the international temperature scale of 1990 (ITS-90).¹² The emissivity ϵ for the Na-HPBB has been determined to be 0.9992,¹³ and the uncertainty¹⁴ in the temperature calibration is 0.62 °C.¹⁵ Further details of the Na-HPBB are available elsewhere.¹³

The Na-HPBB was stabilized at a preset temperature by controlling the pressure of the helium gas (and thus the dew point temperature of the Na vapor). Immediately before and after each data point, a background measurement was acquired by blocking the aperture of the blackbody using several layers of cardboard at ambient temperature. The cardboard had air between each layer to prevent the layer of cardboard facing the spectrograph from heating during the background measurement. The data were accepted if the background images obtained before and after data collection displayed negligible variation. To profile the blackbody aperture, the vertical line imaged by the spectrograph was scanned horizontally across the 22 mm aperture diameter by moving the spectrograph in 2 mm increments.

The position axis of the CCD array was calibrated by imaging a precisely positioned wire suspended horizontally in front of the blackbody aperture at predetermined locations. The wire resulted in a single row of pixels being shadowed, and thus the location of the wire could be inferred from the location of the pixel row in which the intensity decreased dramatically. A linear calibration was employed to relate the vertical position in millimeters to the pixel columns.

The spectral dimension of the CCD array was calibrated by positioning a narrow band filter in front of the blackbody aperture. The resulting image corresponds to a narrow band of high intensity signal centered at the center wavelength of the filter. Using two narrow band filters, a linear wavelength calibration was developed for each position row of the array.

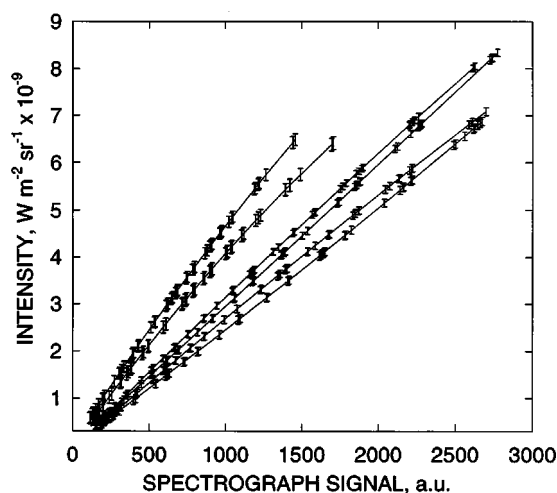


FIG. 3. Intensity calibration at six representative pixels of the PtSi CCD array.

The center wavelength of the narrow band filters were determined to be 2.56 and 4.35 μm using a Fourier transform infrared spectrometer. For each of the filters, the location on the CCD array corresponding to the center wavelength (as determined from the mid point of the peak width at half the maximum height) was determined by linear interpolation. Thus, the wavelength calibration corresponds to subpixel accuracy.

The calibration of the signal intensity (pixel voltage to radiation intensity) was performed by imaging the aperture of the blackbody at various temperatures, and using Planck's law to relate the blackbody temperature to a radiant intensity. Because the spectrograph images a line 35 mm in length and the blackbody aperture is only 22 mm, it was necessary to calibrate the array in three sections. The spectrograph was initially aligned so that the center of the CCD array imaged the center of the aperture. Three images were obtained at this position and used to calibrate the center 1/3 of the array. The spectrograph was then translated 11 mm downward to calibrate the top 1/3 of the array. The bottom 1/3 of the array was calibrated in the same manner. The procedure was repeated for each temperature, and a quadratic function was obtained relating the incident intensity to the pixel voltage at each pixel. Following the initial characterization of the spectrograph with the Na-HPBB, subsequent calibrations were performed using a Mikron⁹ blackbody with a 50.8 mm aperture, thus eliminating the need to perform the calibration in three sections. A sample calibration showing the relationship between signal (in arbitrary units) and radiant intensity is presented in Fig. 3 corresponding to six representative pixels of the CCD array.

The radiance calibration revealed that the transmission characteristics of the spectrograph were poor over the wavelength range from 1.9 to 2.5 μm . Thus, the useful spectral range of the spectrograph is limited to 2.5–5.0 μm . A useful method of presenting the calibration results is to plot the responsivity (ratio of the signal to the radiance) as a function of wavelength, as shown in Fig. 4. The data in Fig. 4 correspond to the 100th position row of the CCD array. Three replicated data sets are presented at each temperature, show-

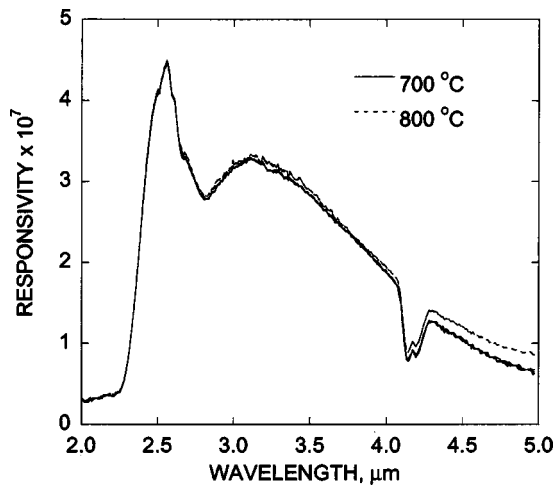


FIG. 4. Responsivity measurements of the infrared spectrograph.

ing excellent repeatability. It should be noted, however, that the responsivity for the two different temperatures matched well below 4 μm , but exhibited a disparity above 4 μm . The disparity is likely due to the nonlinearity of the calibration curves that results from the CCD array and the transmission characteristics of the optics. Note that the variation in the responsivity data presented in Fig. 4 indicate that the uncertainty in the data obtained with the spectrograph will be a function of wavelength. The dips in the responsivity curves near 2.7 and 4.2 μm are a result of absorption by ambient H_2O and CO_2 .

After the calibrations were obtained for the position axis, the spectral axis, and the responsivity, the Na-HPBB aperture was imaged to ensure that the spectrograph data could be used to determine accurately the temperature of the blackbody. The temperature was determined from the data obtained using three methods: (i) one-point pyrometry, (ii) n -point pyrometry with $\epsilon = 1$, and (iii) n -point pyrometry with ϵ unknown. The first approach involves using Planck's law and the intensity calibration to relate the pixel voltage to the blackbody temperature, and thus results in an independent temperature measurement at each pixel. Using this approach, the mean temperature across the aperture was measured to be $\mu = 698.9^\circ\text{C}$ with a standard deviation of $s = 0.88^\circ\text{C}$ when the Na-HPBB temperature was 697.5°C . Thus, the uniformity of the spectrograph expressed as s/μ is 0.13%.

The second two approaches to determine the temperature of the blackbody aperture correspond to fitting the experimental data to Planck's law at each position row. Figure 5(A) presents a comparison of the experimental data at one position row with the theoretical Planck curve assuming the emissivity $\epsilon = 1$. The computed temperature resulting from the least-squares optimization of the Planck function and the experimental data is 698.8°C , which is in excellent agreement with the temperature obtained from the first method. Figure 5(B) presents the results of the third method in which least-squares optimization of the Planck function is performed on the experimental data when both the temperature and emissivity are unknown parameters. In this case, the computed temperature is 693.0°C , which is lower than the

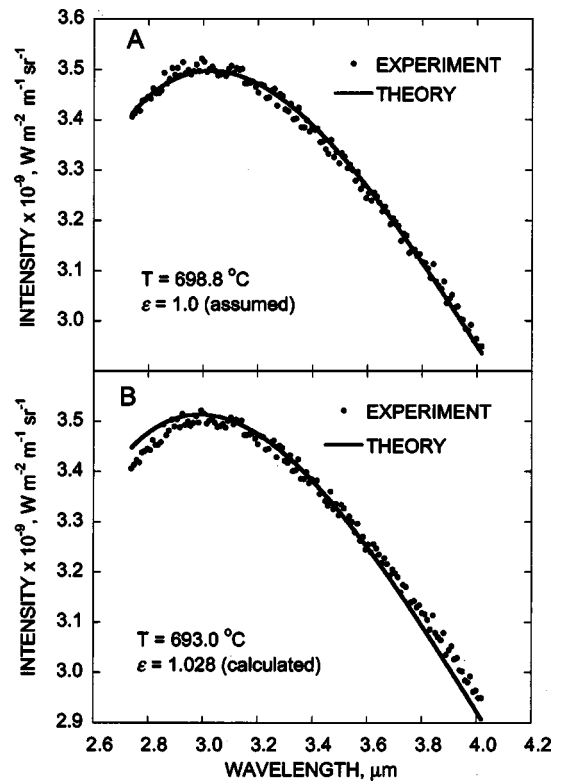


FIG. 5. Comparison of experimental measurement of radiation from the sodium heat pipe blackbody with Planck's curve for the cases of (A) ϵ assumed to be unity and (B) ϵ calculated.

temperature obtained from the other two methods but is within 5°C of the Na-HPBB temperature. The discrepancy between the two approaches in which the data were fit to the Planck function is related to the difficulty in utilizing multi-parameter least-squares optimization techniques for highly nonlinear functions.¹⁶ The above procedure for determining the temperature of the blackbody aperture from the measured emission provides confidence in the spectrograph calibration and assists in the estimation of the uncertainties in the measured extinction coefficients as discussed below.

IV. RESULTS AND DISCUSSION

To determine the extinction coefficient of the soot aerosol, the intensity of radiation reaching the CCD detector from the blackbody is measured with and without aerosol present in the optical cell. Figure 6 presents representative measurements of radiant intensity as a function of wavelength when soot aerosol is and is not present. The blackbody was set at a nominal temperature of 900°C , which provided sufficient intensity without saturating the CCD array when soot was not present. The data in Fig. 6 correspond to the mean measured intensity from approximately 50 to 60 position rows in the center of the aperture image, and the error bars correspond to the standard deviation at each wavelength. The ratio of the two curves in Fig. 6 can be used to calculate the transmission T in Eq. (1). Note that the reliability of the data is compromised in regions of strong gas absorption (e.g., 4.2–4.4 μm). Also, as noted previously, the responsivity of the spectrograph is low below 2.5 μm , which is evident from Fig. 4.

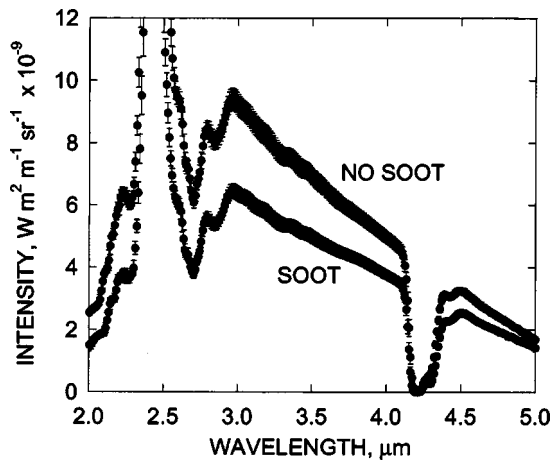


FIG. 6. Measured intensity with and without soot present.

The measurements described above correspond to a steady-state experiment in which the experimental parameters do not vary with time. However, there is one time-varying aspect of the experiment that must be considered when interpreting the data. Due to soot deposition on the windows of the optical cell that occurs during the course of the measurement, the radiation extinction increases with time. This is illustrated in Fig. 7, where the normalized radiant intensity is presented with respect to time. The radiant intensity has been normalized by the first data point (time $t < 0$). The data in the figure correspond to the mean measured intensity of five position rows in the center of the CCD array. The filled diamonds correspond to data obtained when soot was not introduced into the cell, and show the steadiness of the measurement. The solid circles correspond to experimental data obtained when soot was introduced into the optical cell at time zero, but the sedimentation cell shown in Fig. 1 was not in line. The data obtained without the sedimentation cell show a marked decrease in radiant intensity with time due to soot deposition. To calculate the intensity with the soot present, a line was fit through the experimental data (neglecting the first point at $t < 0$) and extrapolated to time zero. The extrapolated value of the radiant intensity was

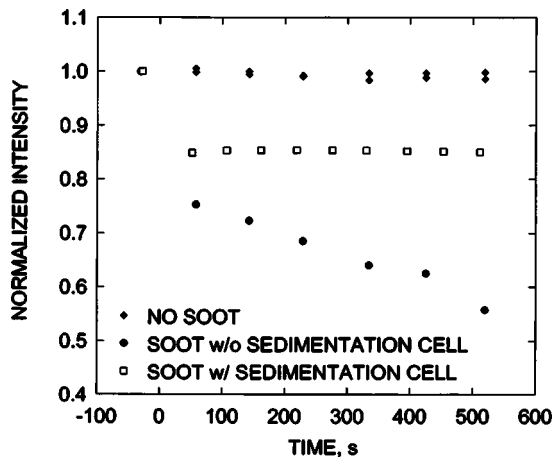


FIG. 7. Effect of soot deposition on the windows of the optical cell. Open and filled squares correspond to data obtained with and without the sedimentation cell, respectively.

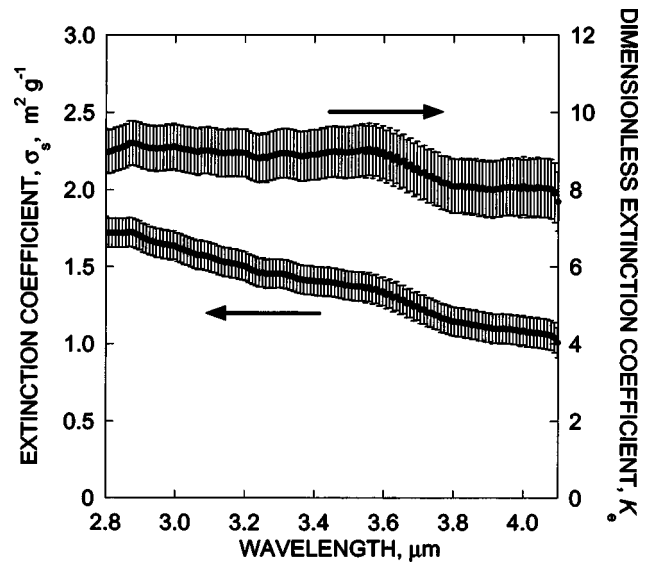


FIG. 8. Calculated values of the mass specific extinction coefficient σ_s and the dimensionless extinction coefficient K_e .

then used to calculate the transmission. The infrared spectrograph described herein permits data over a range of wavelengths to be rapidly obtained, which is essential when there is non-negligible soot deposition on the windows. An experimental apparatus that requires a long time to collect data, such as a scanning monochromator, would not be suitable for such a time-varying experiment.

The open squares symbols correspond to data obtained with the sedimentation cell. The sedimentation cell, which greatly improves the reproducibility of the gravimetric measurements by removing the largest soot agglomerates from the aerosol dispersion, also reduces the soot deposition on the windows. The improvement in the gravimetric measurements and decrease in soot deposition on the windows comes at a cost, however, as the decrease in intensity due to extinction by the aerosol is less with the sedimentation cell present. This results in increased uncertainty in the extinction measurement. However, this can be remedied by increasing the path length L or increasing the mass concentration m_s of particulate (by decreasing the flow rate of N_2).

Figure 8 presents the calculated mass extinction coefficient σ_s and the dimensionless extinction coefficient K_e obtained from the experimental data. Note that the sedimentation cell was used in the measurements presented. The mean soot concentrations obtained from the gravimetric measurements were 0.356 ± 0.036 and 0.262 ± 0.012 $g\ m^{-3}$ for filters 1 and 2, respectively. The uncertainty reported here corresponds to the standard deviation of replicated measurements. The dimensionless extinction coefficient was obtained from Eq. (2) using a value of $\rho_s = 1860$ $g\ m^{-3}$ for the density of the soot particles³ and the mean soot concentration obtained from the upstream and downstream filters. Tables I and II present the individual components of the uncertainty analysis for the calculated mass specific extinction coefficient and dimensionless extinction coefficient, respectively.

The extinction coefficients presented in Fig. 8 represent the first reported measurements in this wavelength region. However, the dimensionless extinction coefficients K_e can be

TABLE I. Uncertainty budget for the mass specific extinction coefficient σ_s ($\phi=1$, $\lambda=3.5 \mu\text{m}$).

Source of uncertainty	Standard uncertainty ($\text{m}^2 \text{g}^{-1}$)	
	Type A	Type B
Intensity ratio, I/I_0	0.022	...
Wavelength λ	...	0.014
Pathlength L	...	0.0073
Mass concentration of soot m_s
Optical cell temperature	...	0.013
Soot losses in optical cell	...	0.0069
Filter weight	0.084	...
Collection time	...	0.023
Gas flow rate	...	0.0069
Combined standard uncertainty ($k=2$): $0.186 \text{ m}^2 \text{g}^{-1}$		

compared with measurements obtained at visible and near-infrared wavelengths. Zhu *et al.*¹⁷ measured K_e of soot in the postflame region produced by the laminar burning of ethene and acetylene. The values are reported for wavelengths of 543.5, 632.8, 856, 1314, and 1565 nm. For ethene the K_e varies slightly with wavelength with a minimum value of 9.17 and a maximum of 9.62. For acetylene, K_e increases monotonically with wavelength from 7.95 at 543.5 nm to 10.0 at 1565 nm. The nominal expanded uncertainty (95% confidence interval) is ± 0.50 . The experiments of Zhu *et al.*¹⁷ are for overventilated burning with the air flow rate at least ten times higher than required for complete combustion, while for the current experiment the air flow is just sufficient for stoichiometric burning with an equivalence ratio of 1.0 so that the properties of the soot may be somewhat different. However, previous measurements by Leonard *et al.*¹⁸ of the morphology and organic/graphitic character of the soot at an equivalence ratio of 1.0 for ethene fuel for the same burner indicate similar characteristics in terms of the agglomerate structure and high graphitic content to that observed for soot produced in more overventilated conditions.

The symbols in Fig. 8 correspond to the mean extinction coefficients obtained from numerous replicated measurements, and the error bars correspond to the combined standard uncertainty (coverage factor, $k=1$). The uncertainty estimates include type A and B uncertainties, and account for variations between replicated measurements and uncertainties that cannot be quantified using statistical methods.^{19,20} The uncertainty estimate includes contributions from the measurement of soot concentration, radiation intensity, and wavelength. The dominant source of uncertainty in the re-

TABLE II. Uncertainty budget for the dimensionless extinction coefficient K_e ($\phi=1$, $\lambda=3.5 \mu\text{m}$).

Source of uncertainty	Standard uncertainty ($\text{m}^2 \text{g}^{-1}$)	
	Type A	Type B
Mass specific extinction coefficient σ_s	...	0.61
Condensed phase soot density ρ_s	...	0.27
Wavelength λ	...	0.090
Combined standard uncertainty ($k=2$): 1.34		

ported extinction coefficients is due to the uncertainty in the gravimetric measurements, which results from soot losses in the optical cell and tubing, and uncertainties in the collection time and total flow during the measurements. As noted above, the uncertainty in the measurements varies with wavelength due to the wavelength dependence of the responsivity of the infrared spectrograph. In particular, the uncertainty increases outside the wavelength range of 2.8–4.0 μm . Within the wavelength range of 2.8–4.0 μm , the combined standard uncertainty is approximately $\pm 10\%$ of the reported value of the extinction coefficient.

In summary, an experimental apparatus has been presented to measure the mass specific extinction coefficient of post-flame soot aerosol in the wavelength range of 2.5–5.0 μm , with the lowest uncertainties corresponding to the range 2.8 $\mu\text{m} < \lambda < 4.0 \mu\text{m}$. This wavelength range represents a critical range for the prediction of radiation transport in fires, and has not been previously explored. The infrared spectrograph permits the rapid collection of extinction data over a range of wavelengths, which would not be feasible using other techniques.

ACKNOWLEDGMENTS

The authors would like to acknowledge the assistance of Marco Fernandez with the assembly of the experimental apparatus. They would also like to thank Tyler Smith, a student intern in their laboratory, for his help with the spectroscopic and gravimetric measurements. They are also indebted to Carol Johnson for many helpful discussions, and to Paul Fuss for characterization of the narrow band filters used. The infrared spectrograph discussed herein was developed by En'Urga Inc. as part of a Phase II SBIR grant from NIST.¹⁰

¹H. R. Baum, K. B. McGrattan, and R. G. Rehm, *J. Heat Transfer Soc. Jpn.* **35**, 45 (1997).

²K. B. McGrattan, H. R. Baum, and R. G. Rehm, *Fire Saf. J.* **30**, 161 (1998).

³R. A. Dobbins, G. W. Mulholland, and N. P. Bryner, *Atmos. Environ.* **28**, 889 (1994).

⁴M. Y. Choi, G. W. Mulholland, A. Hamins, and T. Kashiwagi, *Combust. Flame* **102**, 161 (1995).

⁵I. Colbeck, B. Atkinson, and Y. Johar, *J. Aerosol Sci.* **28**, 715 (1997).

⁶G. W. Mulholland and M. Y. Choi, 27th Symposium (International) on Combustion—The Combustion Institute, 1998, Vol. 27, p. 1515.

⁷J. Zhu, M. Y. Choi, G. W. Mulholland, and L. A. Gritzo, *Proceedings of the Combustion Institute*, 2000, Vol. 28, p. 439.

⁸J. Zhu, M. Y. Choi, G. W. Mulholland, and L. A. Gritzo, *Int. J. Heat Mass Transf.* **43**, 4399 (2000).

⁹Certain commercial equipment, instruments, or materials are identified in this article to specify adequately the experimental procedure. Such identification does not imply recommendation or endorsement by the National Institute of Standards and Technology, nor does it imply that the materials or equipment are necessarily the best available for this purpose.

¹⁰Y. Sivathanu, R. Joseph, J. Lim, Y. Zheng, and J. Gore, NIST Report No. GCR 99-777, 1999.

¹¹J. Ji, J. P. Gore, Y. R. Sivathanu, and J. Lim, *Proceedings of NHTC 2000*, 34th National Heat Transfer Conference, Pittsburgh, PA, 2000.

¹²H. Preston-Thomas, *Metrologia* **27**, 3 (1990).

¹³F. J. Lovas, B. K. Tsai, and C. E. Gibson, *Mater. Res. Soc. Symp. Proc.* **525**, 127 (1998).

¹⁴Unless otherwise specified, all uncertainties reported herein correspond to a combined expanded uncertainty with a coverage factor of $k=2$, which corresponds approximately to a 95% confidence interval.

¹⁵B. K. Tsia, J. F. Widmann, M. Bundy, and S. M. Hill, *Proceedings of*

Thermosense XXIII—SPIE—The International Society of Optical Engineering, Orlando, FL, 2001.

¹⁶G. Neuer, L. Fiessler, M. Groll, and E. Schreiber, *Temperature—Its Measurement and Control in Science and Industry* (1992), Vol. 6, p. 787.

¹⁷J. Zhu, M. Y. Choi, M. Young, G. W. Mulholland, and L. A. Gritzo,

Proceedings of the Combustion Institute, 2002 (accepted for publication).

¹⁸S. Leonard, G. W. Mulholland, R. Puri, and R. J. Santoro, *Combust. Flame* **98**, 20 (1994).

¹⁹B. N. Taylor and C. E. Kuyatt, NIST Technical Note No. 1297, 1984.

²⁰ANSI/NCSL Report No. Z540-2-1997, 1997.